Research on Pilot Control Strategy and Workload for Tilt-Rotor Aircraft Conversion Procedure

Xufei Yan , Ye Yuan * , Renliang Chen

Posted Date: 29 June 2023

doi: 10.20944/preprints202306.2005.v1

Keywords: tilt-rotor; conversion; optimal control model; pilot workload; wavelet transform

Article

Research on Pilot Control Strategy and Workload for Tilt-Rotor Aircraft Conversion Procedure

Xufei Yan [1], Ye Yuan [2,*] and Renliang Chen [3]

[1] Zhejiang Lab, Hangzhou 311100, China; yanxufei@zhejianglab.com
[2] Swansea University, Wales SA2 8PP, UK
[3] Nanjing University of Aeronautics and Astronautics, Nanjing 210016, China; crlae@nuaa.edu.cn
* Correspondence: ye.yuan@swansea.ac.uk

Abstract: This paper studies the pilot control strategy and workload of tilt-rotor aircraft dynamic conversion procedure between helicopter mode and fixed-wing mode. A nonlinear flight dynamics model of tilt-rotor aircraft with full flight modes is established. On this basis, a nonlinear optimal control model of dynamic conversion is constructed, considering factors such as conversion corridor limitations, pilot control, flight attitude, engine rated power, and wing stall effects. To assess pilot workload, an analytical method based on wavelet transform is proposed, which examines the mapping relationship between pilot control input's amplitude, constituent frequencies, and control tasks. By integrating the nonlinear optimal control model and the pilot workload evaluation method, the analysis of pilot control strategy and workload during the conversion procedure is conducted, leading to the identification of strategies to reduce pilot workload. The results indicate that incorporating the item of pilot workload in the performance index results in a notable reduction in the magnitude of collective stick inputs and longitudinal stick inputs. Moreover, it facilitates smoother adjustments in altitude and pitch attitude. Additionally, the conversion of the engine nacelle can be achieved at a lower and constant angular velocity. In summary, the conversion and reconversion procedures are estimated to have a low workload (Level 1 ~ Level 2), with relatively simple and easy manipulation for the pilot.

Keywords: tilt-rotor; conversion; optimal control model; pilot workload; wavelet transform

1. Introduction

The tilt-rotor aircraft combines the capabilities of helicopter vertical takeoff and landing as well as the fixed-wing aircraft high speed and range. It consists of three flight modes that are helicopter mode, fixed-wing aircraft mode and conversion mode. Conversion between helicopter mode and fixed-wing aircraft mode is completed by tilting the nacelle of the engine [1].

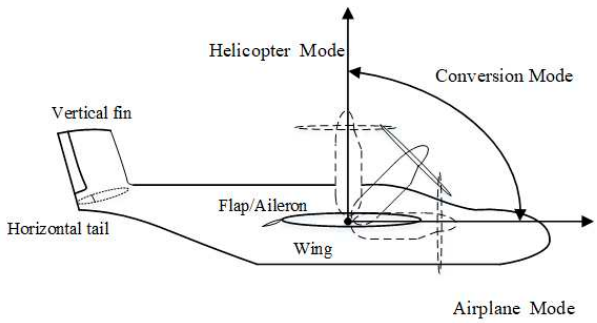

Figure 1. XV-15 tilt-rotor aircraft conversion flight mode.

The control process during conversion is complicated because of the cooperation between the lift and thrust, complex unsteady aerodynamic effects, body motion and inertial coupling as well as the control transition between helicopter mode and fixed-wing mode [2–4]. In the conversion

procedure, the pilot not only has to focus on cockpit control but also pay attention to the tilting of the nacelles, which significantly increases the pilot workload [5,6].

Several studies have investigated the pilot control strategy during the conversion procedures of tilt-rotor aircraft between helicopter mode and fixed-wing mode [5–7]. Righetti conducted simulations of conversion maneuvers in order to minimize pilot workload [7]. However, the optimization results may be limited by a predetermined conversion path and nacelle tilting schedule, potentially leading to suboptimal outcomes. Yan transformed the pilot control strategy optimization problem during the conversion procedure into a Nonlinear Optimal Control Problem (NOCP) to relieve the pilot workload [5]. By studying the influence of different conversion paths on pitch attitude, altitude and the power required during the conversion procedure, Yeo sought a better conversion path to improve flight attitude and mitigate altitude variations [6]. The aforementioned studies have proposed control methods aimed at reducing the pilot workload through research and optimization of pilot control strategies based on high-precision flight dynamics models. However, these studies have primarily focused on qualitative analysis of pilot smooth control, without further quantification and evaluation of the pilot workload involved. Therefore, it is necessary to conduct additional research to quantify and analyze the pilot workload in order to provide a comprehensive understanding of the topic.

Recent research on quantifying pilot control workload has focused on methods that describe the temporal characteristics of control actions. Memon and Padfield [8] utilized wavelet transform analysis to extract frequency and amplitude information from flight test data. Bachelder and Aponso et al. [9] applied time-frequency scale maps obtained through wavelet analysis to calculate time-varying cutoff frequencies to quantify pilot control workload. They demonstrated that these frequencies are likely correlated with pilot HQR ratings in flight tests [10]. Klyde et al. [11,12] applied various pilot control action analysis methods to analyze pilot control actions. The results indicated that relying solely on cutoff frequency to derive pilot workload can be misleading. Conversely, the major frequency components obtained through multi-frequency component analysis align closely with the descriptions provided by pilots and offer additional information on control frequencies and energy. From the above research, it can be observed that pilot control action analysis methods based on time-frequency representations (TFRs) can more accurately quantify and assess pilot control workload. However, currently, there is a lack of established metrics for accurately quantifying pilot workload in the research of tilt-rotor aircraft conversion control strategy optimization.

Therefore, this paper first employs nonlinear optimal control theory to establish a dynamic conversion optimal control model and designs an efficient numerical solution method to obtain the trajectory and control strategy. Subsequently, a pilot workload evaluation method based on wavelet transform is developed to provide metrics for pilot workload assessment. This approach helps in identifying control strategies that are more reasonable and effective in alleviating pilot burden. The XV-15 tilt-rotor aircraft is taken as the example.

In section 2, a nonlinear rigid body dynamics model of the XV-15 tilt rotor aircraft is established and verified with flight data. In section 3, a nonlinear optimal control model of dynamic conversion is constructed in the form of performance index, path constraints and boundary conditions. An efficient numerical solution method with good convergence is designed to obtain the trajectory and control strategy. In section 4, this paper propose a pilot control workload evaluation method utilizing wavelet transform. This method considers the mapping relationship between pilot control magnitude, frequency components, and control difficulty. Finally, in sections 5 and 6, the pilot control strategy, flight state and pilot workload during forward conversion and backward reconversion procedures are compared and discussed under different performance indexes. Conclusions are given in section 7.

Preprints (www.preprints.org) | NOT PEER-REVIEWED | Posted: 29 June 2023 doi:10.20944/preprints202306.2005.v1

2. Flight dynamics model of XV-15 tilt-rotor aircraft

2.1. Modelling

In this paper, a XV-15 tilt-rotor aircraft is utilized as a sample. The nonlinear flight dynamics model of XV-15 tilt-rotor aircraft [1] consists of two rotor models, a wing-pylon model, a fuselage model, a horizontal stabilizer model, a vertical stabilizer model and a mixed control system. A brief introduction of the model is given below,

1. The aerodynamic forces and moments acting on the rotors are calculated using blade element theory. For each blade element, lift, drag and moment are calculated using table look-up method to account for flow separation and transonic compressibility effects.

2. The Pitt-Peters dynamic inflow model with rotor wake distortion effect and side-by-side rotor effect is applied to simulate the dynamic characteristics of rotor inflow during tilting [13].

3. The calculation of the wing aerodynamic forces and moments due to rotor wake effects is made separately from the forces and moments generated by the freestream flow. The effect of rotor wake on the wing is a function of contracted wake radius, tilting angle, angle of attack, angle of sideslip, and dynamic pressure of the portion of the wing immersed in the wake, see details in GTRS model Ref. [14].

4. The fuselage, wing-pylon assembly, horizontal tail and vertical fins are modelled separately in order to facilitate accounting for the influence of rotor wake on the airframe aerodynamics, see details in GTRS model Ref. [14].

Finally, according to the influence of nacelle tilting motion on rotor aerodynamics, the interference between aerodynamic components and the inertial coupling during dynamic conversion as well as the characteristics of control transition between helicopter mode and fixed-wing mode [14], a nonlinear flight dynamics model of tilt-rotor aircraft with full flight modes is established as follows

$$\dot{\boldsymbol{x}}_b = f(\boldsymbol{x}_b, \boldsymbol{u}_b, t) \tag{1}$$

where $\boldsymbol{x}_b = [\boldsymbol{x}_\mathrm{B}; \boldsymbol{x}_\mathrm{F}; \boldsymbol{x}_\mathrm{I}]$ represents the state vector. It contains the fuselage state $\boldsymbol{x}_\mathrm{B}$, the rotor state $\boldsymbol{x}_\mathrm{F}$ (Left and Right), and inflow state $\boldsymbol{x}_\mathrm{I}$. $\boldsymbol{u}_b = \left[\delta_\mathrm{col}; \delta_\mathrm{lon}; \delta_\mathrm{lat}; \delta_\mathrm{ped}; i_\mathrm{n}\right]$ is the control vector, in which δ_col is the collective stick input, δ_lat is the lateral stick input, δ_lon is the longitudinal stick input, δ_ped is the pedal input, the nacelle tilting angle i_n is applied to study the engine nacelle tilting law which can be realized by automatic tilting system, t is the time.

$$\begin{cases} \boldsymbol{x}_\mathrm{B} = [u, v, w, p, q, r, \phi, \theta, \psi, x, y, h]^\mathrm{T} \\ \boldsymbol{x}_\mathrm{F} = \left[\dot{a}_{0,\mathrm{R}}, \dot{a}_{1,\mathrm{R}}, \dot{b}_{1,\mathrm{R}}, a_{0,\mathrm{R}}, a_{1,\mathrm{R}}, b_{1,\mathrm{R}}, \dot{a}_{0,\mathrm{L}}, \dot{a}_{1,\mathrm{L}}, \dot{b}_{1,\mathrm{L}}, a_{0,\mathrm{L}}, a_{1,\mathrm{L}}, b_{1,\mathrm{L}}\right]^\mathrm{T} \\ \boldsymbol{x}_\mathrm{I} = \left[\nu_{0,\mathrm{R}}, \nu_{1\mathrm{s},\mathrm{R}}, \nu_{1\mathrm{c},\mathrm{R}}, \nu_{0,\mathrm{L}}, \nu_{1\mathrm{s},\mathrm{L}}, \nu_{1\mathrm{c},\mathrm{L}}\right]^\mathrm{T} \end{cases} \tag{2}$$

where u, v, w represent the linear velocities of the aircraft body axis system, p, q, r correspond to the angular velocities of the body axis system, ϕ, θ, ψ represent roll, pitch and yaw angles, x, y, h denote the position of the aircraft in the Earth axis system. a_0, a_1, b_1 denote the taper, rear, and side angles of the rotor disk, respectively. $\nu_0, \nu_{1\mathrm{c}}, \nu_{1\mathrm{s}}$ represent the non-dimensional terms for rotor uniform inflow, first-order cosine inflow, and first-order sine inflow, respectively.

2.2. Validation

The flight test data of XV-15 tilt-rotor aircraft (gross weight of 5897 kg) is utilized as a sample for steady-state analysis in three modes of flight. Figures 2 and 3 show the comparison between the predicted results and the flight test data [15]. Figure 3 shows the collective pitch angle, longitudinal stick displacement, vehicle pitch attitude and total power required against the flight test data for

Preprints (www.preprints.org) | NOT PEER-REVIEWED | Posted: 29 June 2023 doi:10.20944/preprints202306.2005.v1

helicopter mode ($i_n = 90^\circ$) with Flaps/Ailerons setting of $40^\circ / 25^\circ$, conversion mode ($i_n = 60^\circ$ and $i_n = 30^\circ$) with Flaps/Ailerons setting of $20^\circ / 12.5^\circ$ as well as the fixed wing aircraft mode ($i_n = 0^\circ$) with Flaps/Ailerons setting of $0^\circ / 0^\circ$. It can be seen that the steady-state variables calculated are in good agreement with the flight test data.

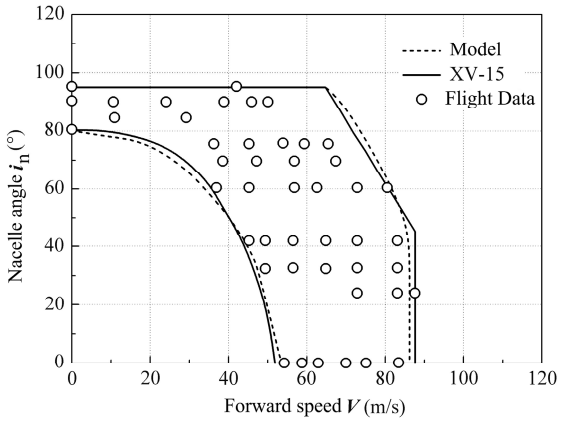

Figure 2. Conversion corridor of XV-15 tilt-rotor aircraft.

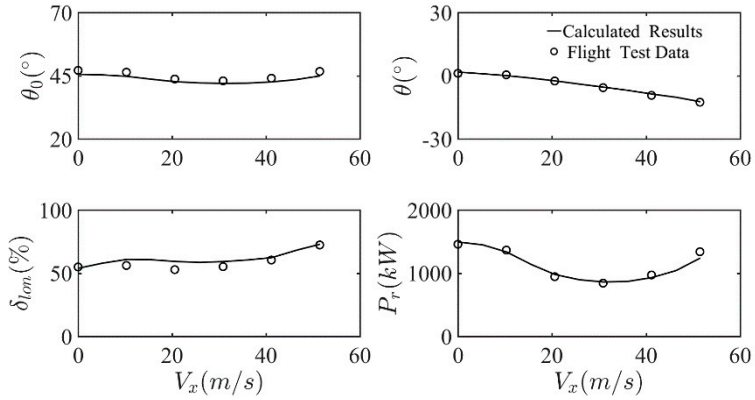

(a) i_n=90°, 40°/25°

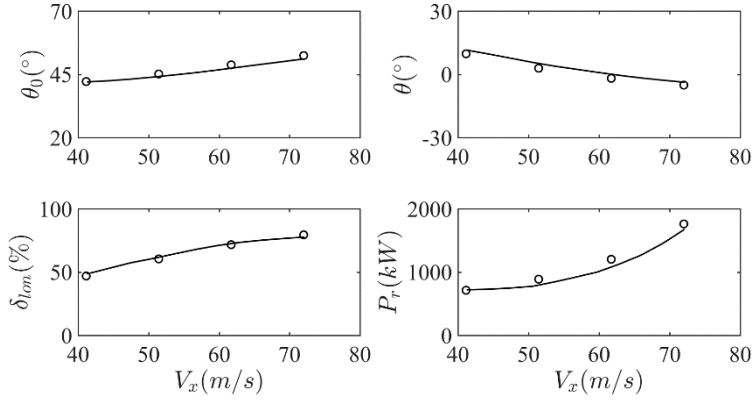

(b) i_n=60°, 20°/12.5°

Preprints (www.preprints.org) | NOT PEER-REVIEWED | Posted: 29 June 2023 doi:10.20944/preprints202306.2005.v1

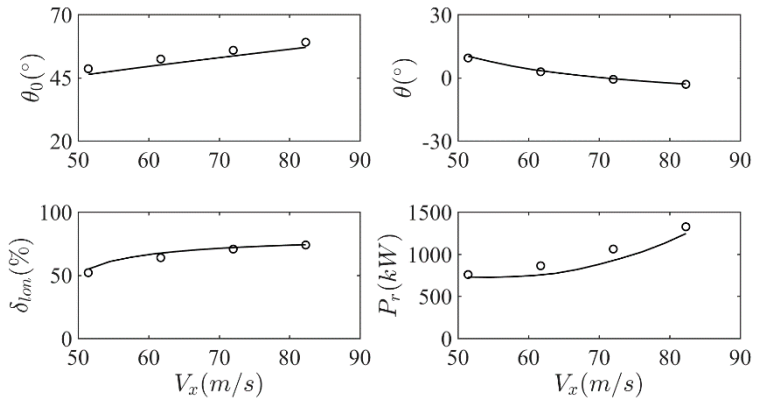

(c) i_n=30°, 20°/12.5°

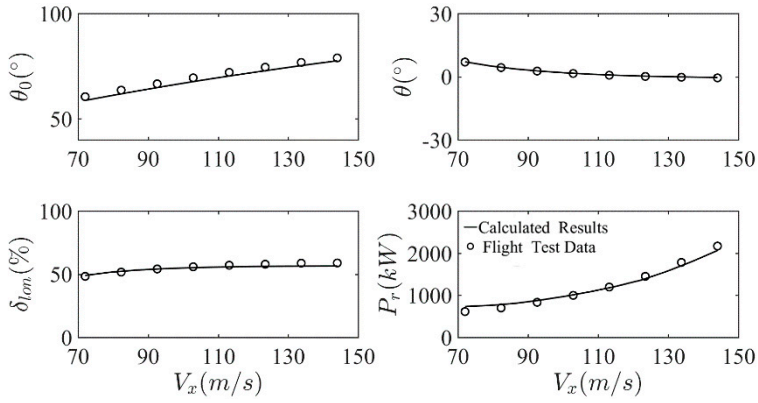

(d) i_n=0°, 0°/0°

Figure 3. Comparison of the calculated trim results with flight data.

3. Formulation of nonlinear optimal control problem

3.1. Nonlinear optimal control problem

Based on the flight dynamics model and the characteristics of conversion between helicopter mode and fixed-wing aircraft mode, the tilt-rotor aircraft conversion procedure is formulated into a nonlinear optimal control problem (NOCP), which can be expressed as follows [5,16].

1) *Differential equations*: Which is basically the flight dynamics model. In order to account for the limits on the control rates of pilot control inputs as well as the nacelle angle, and to avoid jump discontinuities arising in the time history of controls in the control optimization, time derivatives of $\delta_{\text{col}},\delta_{\text{lon}},\delta_{\text{lat}},\delta_{\text{ped}},i_{\text{n}}$ are applied as the control variables, denoted by $u_{\text{c}},u_{\text{lon}},u_{\text{lat}},u_{\text{ped}},u_{\text{n}}$. In the meantime, $\delta_{\text{col}},\delta_{\text{lon}},\delta_{\text{lat}},\delta_{\text{ped}},i_{\text{n}}$ are regarded as the state variables. The corresponding differential equations can be expressed as

$$\dot{\boldsymbol{x}} = f\left(\boldsymbol{x},\boldsymbol{u},t\right) \tag{3}$$

where

$$\begin{cases} \boldsymbol{x} = \left[\boldsymbol{x}_{\text{B}};\boldsymbol{x}_{\text{F}};\boldsymbol{x}_{\text{I}};\boldsymbol{u}_b\right] \\ \boldsymbol{u} = \left[u_{\text{col}},u_{\text{lon}},u_{\text{lat}},u_{\text{ped}},u_{\text{n}}\right]^{\text{T}} \end{cases} \tag{4}$$

The tilt-rotor aircraft has a longitudinally symmetrical configuration, thus the conversion procedure is in the longitudinal plane under no crosswind conditions. In order to improve the calculation efficiency of the nonlinear optimal control method, this paper assumes that the state variables and control variables related to lateral and heading motion in the flight dynamics model remain in the initial state, and do not participate in the numerical calculation of dynamic conversion.

Preprints (www.preprints.org) | NOT PEER-REVIEWED | Posted: 29 June 2023 doi:10.20944/preprints202306.2005.v1

2) *Optimal variables*: Differential state variables $\boldsymbol{x}$, control variables $\boldsymbol{u}$, and the free final time t_f (with the initial time t_0 set to 0).

3) *Cost function*: The cost function of the NOCP is the performance index of the whole conversion procedure, which needs to consider the influence of multiple factors, such as the time of dynamic conversion, flight safety, feasibility and pilot workload, etc. Hence the cost function J can be formulated into the following general expression

$$\min_{\boldsymbol{u}} J = \phi\left(\boldsymbol{x}(t_0), t_0, \boldsymbol{x}(t_\mathrm{f}), t_\mathrm{f}\right) + \int_{t_0}^{t_\mathrm{f}} L\left(\boldsymbol{x}(t), \boldsymbol{u}(t), t\right) dt \tag{5}$$

where t_0 is the fixed initial time, t_f is the free terminal time. The first term of expression Equation (5) represents the initial and terminal state performance index, and the second term represents the state and control performance index of the whole conversion procedure. The specific cost function will be given in Sections 5 and 6. The NOCP can be successfully solved if the time history of the control vector $\boldsymbol{u}(t)$ that minimizes the cost function is found under the following constraints.

4) *Constraints*: The constraint equations consist of initial boundary conditions, path constraints and terminal constraints.

The initial boundary conditions are the current flight state of the aircraft. The terminal constraints are set as the target tilting angle and forward flying speed

$$\begin{cases} i_\mathrm{n}(t_\mathrm{f}) = i_\mathrm{nt} \\ u_\mathrm{n}(t_\mathrm{f}) = 0°/\mathrm{s} \\ \dot{x}_{\mathrm{t,min}} \le \dot{x}(t_\mathrm{f}) \le \dot{x}_{\mathrm{t,max}} \\ \dot{h}_{\mathrm{t,min}} \le \dot{h}(t_\mathrm{f}) \le \dot{h}_{\mathrm{t,max}} \end{cases} \tag{6}$$

where i_{nt} is the target engine nacelle tilting angle, $\dot{x}_\mathrm{t}$ is the target forward speed, $\dot{h}_\mathrm{t}$ is the target ascent rate, the specific values and additional items can be determined according to the requirements of the conversion flight mission.

The path constraints should be determined by the boundary of conversion corridor as shown in Figure 2. In low-speed conversion, the lift provided by the wing is limited by the critical stall angle of attack. Therefore, the wing angle of attack is at the critical value in the lower conversion envelope. The corresponding path constraint is

$$\alpha_{\mathrm{WC,min}} \le \alpha_\mathrm{W}(t) \le \alpha_{\mathrm{WC,max}} \tag{7}$$

where the critical angle of attack $\alpha_{\mathrm{WC,min}}$ and $\alpha_{\mathrm{WC,max}}$ can be obtained from wind tunnel data [14]. The maximum forward speed in the conversion procedure is limited by the compressibility of the advancing rotor blade, the stall effect of the retreating rotor blade, the available power and dynamic stability of the rotor, among which the available power of the rotor is dominant. Therefore, the path constraint determined by the upper conversion envelope is

$$0 \le P_\mathrm{r}(t) \le P_\mathrm{n} \tag{8}$$

where P_n represents the rated power output of the engine (two). In order to further ensure the flight safety during the conversion process, the speed corresponding to the engine nacelle tilting angle of 45° on the upper conversion envelope is taken as the stop speed, and the flight speed during the conversion process shall not exceeds the stop speed V_{stop}.

$$V_{\max} \le V_{\mathrm{stop}} \tag{9}$$

In addition, the constraints of altitude, pitch attitude as well as the pilot control inputs should also be considered in the path constraints. Notice that in order to study the influence of pilot control strategy on height change during dynamic conversion, the height constraint is appropriately relaxed. The constraints of control rates are selected according to the maximum physical rate limits of the servo booster.

Preprints (www.preprints.org) | NOT PEER-REVIEWED | Posted: 29 June 2023 doi:10.20944/preprints202306.2005.v1

$$\begin{cases} \Delta h_{\min} \le \Delta h(t) \le \Delta h_{\max} \\ -10^\circ \le \theta(t) \le 10^\circ \\ -5^\circ/\mathrm{s} \le q(t) \le 5^\circ/\mathrm{s} \end{cases} \tag{10}$$

$$\begin{cases} 0 \le \delta_{\mathrm{col}}(t), \delta_{\mathrm{lon}}(t) \le 1, 0^\circ \le i_{\mathrm{n}}(t) \le 90^\circ \\ -0.3/\mathrm{s} \le u_{\mathrm{col}}(t), u_{\mathrm{lon}}(t) \le 0.3/\mathrm{s} \\ -15^\circ/\mathrm{s} \le u_{\mathrm{n}}(t) \le 15^\circ/\mathrm{s} \end{cases} \tag{11}$$

3.2. Numerical solution techniques

The state and control variables of the NOCP for XV-15 tilt-rotor aircraft conversion procedure are numerous, and the cost function as well as the constraints are very complicated. Therefore, the optimal solution needs to be solved numerically. To improve computational efficiency and rate of convergence in the numerical optimization, the optimal variables of the NOCP are normalized and scaled first as follows

$$\begin{cases} (\bar{u},\bar{v},\bar{w}) = \dfrac{k_1}{\Omega_0 R}(u,v,w), \quad (\bar{p},\bar{q},\bar{r}) = \dfrac{k_2}{\Omega_0}(p,q,r) \\ \left(\bar{\dot{a}}_{0,\mathrm{LR}}, \bar{\dot{a}}_{1,\mathrm{LR}}, \bar{\dot{b}}_{1,\mathrm{LR}}\right) = \dfrac{k_2}{\Omega_0}\left(\dot{a}_{0,\mathrm{LR}}, \dot{a}_{1,\mathrm{LR}}, \dot{b}_{1,\mathrm{LR}}\right), \quad (\bar{x},\bar{y},\bar{h}) = \dfrac{k_3}{R}(x,y,h) \\ \bar{\Omega} = \dfrac{\Omega}{\Omega_0}, \quad \tau = k_4\Omega_0 t, \quad \dfrac{d(\bullet)}{d\tau} = \dfrac{1}{k_4\Omega_0}\dfrac{d(\bullet)}{dt} \end{cases} \tag{12}$$

where Ω_0 is the standard main rotor rotational speed, $k_1 \sim k_4$ are the constant scaling factors. In order to make the normalized-scaled optimal variables close to one in value, take k_1=k_2=100, k_3=1, k_4=0.01. The governing equations of the normalized and scaled flight dynamics model can be expressed as

$$\frac{\mathrm{d}\bar{\boldsymbol{x}}}{\mathrm{d}\tau} = f(\bar{\boldsymbol{x}}, \bar{\boldsymbol{u}}, \tau) \tag{13}$$

At present, the most effective and flexible approach to solve NOCP is to convert the NOCP into a nonlinear programming problem (NLP) via a collocation approach, which can be then solved with nonlinear programming algorithm. In this paper, a collection approach called direct multiple shooting [17] is applied to transcribe the NOCP directly into a discrete NLP by breaking the states and controls of the continuous conversion procedure into shorter time segments. This approach is typically used in the applications of high complexity and/or a large number of degrees of freedom [18]. The fundamental idea of direct multiple shooting approach is shown in Figure 4.

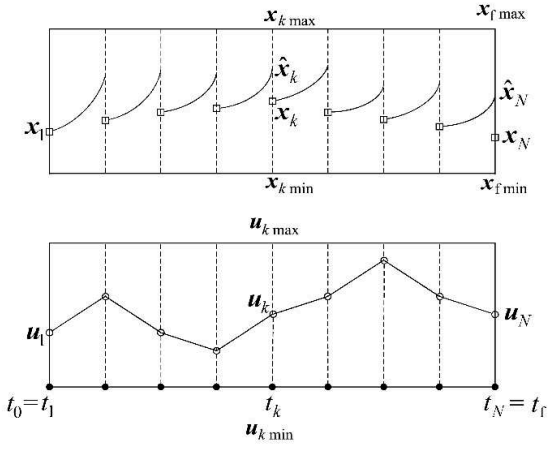

Figure 4. Direct multiple shooting approach.

Preprints (www.preprints.org) | NOT PEER-REVIEWED | Posted: 29 June 2023 doi:10.20944/preprints202306.2005.v1

As can be seen in Figure 4, the solution time interval [τ_0, τ_f] of the NOCP is divided into N-1 equal time segments. At the k-th time interval, we can integrate the differential equations from τ_k to the end of the segment at τ_{k+1} using the time stepping approach with piecewise linear interpolation of $\bar{\boldsymbol{u}}_k$ and $\bar{\boldsymbol{u}}_{k+1}$, which helps to decrease the computational cost of finite differencing by increasing the problem sparsity. The multiple shooting segments are used for stabilizing the integration of the vehicle equations of motion. This method guarantees that the discretized model is as close as possible to the original nonlinear model. Denote the result of this integration by $\hat{\bar{\boldsymbol{x}}}_k$, thus the shooting of segment k can be represented by

$$\bar{\boldsymbol{x}}_{k+1} - \hat{\bar{\boldsymbol{x}}}_{k+1} = \boldsymbol{0}, \quad k = 1, \cdots, N-1 \tag{14}$$

where

$$\hat{\bar{\boldsymbol{x}}}_{k+1} = \bar{\boldsymbol{x}}_k + \int_{\tau_k}^{\tau_{k+1}} f(\bar{\boldsymbol{x}}, \bar{\boldsymbol{u}}, \tau) d\tau \tag{15}$$

The cost function of the NOCP is replaced by the performance index of the NLP in the same way

$$\min J = \phi\left(\bar{\boldsymbol{x}}(\tau_1), \tau_1, \bar{\boldsymbol{x}}(\tau_N), \tau_N\right) + \sum_{k=1}^{N-1} \int_{\tau_k}^{\tau_{k+1}} L\left(\bar{\boldsymbol{x}}(\tau), \bar{\boldsymbol{u}}(\tau), \tau\right) d\tau \tag{16}$$

The constraints are enforced on the corresponding time nodes. The nonlinear programming problem can be effectively solved using SQP algorithm [19] to get the approximate solution of the original NOCP. To improve the accuracy of the optimal solution, the optimal state variables $\boldsymbol{x}(t)$ are calculated by integrating the flight dynamics model (3) from t_0 to t_f with piecewise linear interpolation of $\left(\boldsymbol{u}_1, \boldsymbol{u}_2, ..., \boldsymbol{u}_k, ..., \boldsymbol{u}_N\right)$.

4. Workload evaluation method based on wavelet analysis

Due to the limitations in metrics such as pilot aggressiveness and pilot cutoff frequency [8,9], which fail to directly capture the temporal variations in control actions, several new methods based on time-frequency domain representation have been proposed. Among these methods, the most prominent ones include the short time fourier Transform (STFT) and the recently developed wavelet analysis. Because STFT cannot simultaneously consider the needs of frequency and time resolution, the wavelet analysis method with good time-frequency resolution is more widely used in engineering [12]. This paper primarily focuses on studying pilot control actions using wavelet analysis and attempts to evaluate and analyze pilot control workload based on this approach.

Compared to the Power Spectral Density (PSD), the time-frequency domain representation can provide insights into the distribution of signal energy in both the frequency spectrum and the time domain. The wavelet analysis method utilizes finite-length bandpass filters, with a length of $g(t)$ equal to n_c / ω_c seconds, where n_c represents the number of cycles. Each point in the wavelet analysis result $G_{\delta\delta}(\omega, t)$ can be interpreted as the weighted power of the input signal $\delta_x(t)$ at frequency ω_c within a time window of length n_c / ω_c. The "weight" is determined by the wavelet function, which is defined as [20].

$$\int_{-\infty}^{\infty} \psi(t) dt = 0 \tag{17}$$

The choice of wavelet function is crucial in wavelet transformation as different wavelet functions have significant waveform differences. Therefore, selecting an appropriate wavelet function is of great importance. In this section, we analyze the characteristics of wavelet functions and consider specific applications to select a suitable wavelet function. In signal recognition applications, the selection of wavelet functions can be based on the following characteristics [21]:

1. *Support set:* Wavelet functions can be divided into compactly supported and non-compactly supported based on their support length. A higher level of compact support indicates more

 doi:10.20944/preprints202306.2005.v1

concentrated energy, while non-compactly supported wavelets may result in energy loss in the decomposed signal, leading to increased recognition errors. Therefore, when recognizing pilot's manipulation actions, wavelet functions with compact support are generally preferred.

2. *Orthogonality:* Refers to the property of orthogonality between the low-frequency and high-frequency components during wavelet function analysis. Orthogonality is beneficial for the reconstruction of wavelet coefficients and is commonly used in image signal processing.

3. *Regularity:* Describes the smoothness level of a function. Wavelet functions with good regularity help improve the fitting performance between the wavelet basis and the signal, accurately describing the pilot's manipulation characteristics.

4. *Vanishing moments:* Indicates the concentration of energy after wavelet transformation. A higher order of vanishing moments filters the high-frequency components more effectively, indicating stronger denoising capabilities of the wavelet transformation. However, if the order of vanishing moments is too large, useful high-frequency components in the signal may be filtered out.

Considering the characteristics mentioned above and referring to related literature, the Daubechies (db) wavelet functions constructed by Ingrid Daubechies satisfy the requirements for analyzing pilot's manipulation actions. The Daubechies wavelet functions exhibit orthogonality, compact support, good regularity, and suitable orders of vanishing moments [22]. Therefore, in this paper, we adopt the Daubechies wavelet functions for wavelet analysis of pilot's manipulation actions.

Once the wavelet function is determined, the pilot's control time history (instantaneous varying signal) can be subjected to wavelet transformation. The wavelet family can be scaled by a scaling factor s and translated by a parameter u. The scaling factor corresponds to frequency, while the translation parameter corresponds to time. Therefore, the wavelet function and its Fourier transform can be expressed as follow,

$$\begin{cases} \psi_{u,s}(t) = \dfrac{1}{\sqrt{s}}\psi\left(\dfrac{t-u}{s}\right) \\ \hat{\psi}_{u,s}(f) = e^{-i2\pi fu}\sqrt{s}\hat{\psi}(sf) \end{cases} \tag{18}$$

The wavelet transform of the time-varying signal can be expressed as follows,

$$W_y(u,s) = \int_{-\infty}^{\infty} y(t)\psi_{u,s}^*(t)dt = \int_{-\infty}^{\infty} \hat{y}(f)\hat{\psi}_{u,s}^*(f)df \tag{19}$$

where $W_y(u,s)$ is referred to as the wavelet coefficient, and * denotes the conjugate relationship.

From the above equation, it can be observed that when the center frequency of the wavelet is close to certain frequency components in the original signal, the wavelet coefficient takes on maximum values. Therefore, the wavelet function can be seen as a bandpass filter that only allows signals with frequencies close to the center frequency of the wavelet to pass through. During the wavelet transformation process, a series of center frequencies can be obtained by scaling factors, while different time-frequency information of the signal can be detected by translation coefficients. This provides information about the frequencies and amplitudes contained in the signal at different time points. Hence, wavelet analysis can identify multiple dominant frequency components in the pilot's control input.

According to research by Tritschler and O'Connor, these frequency components may represent different flight tasks or control strategies employed by the pilot, as shown in Table 1 [23].

Preprints (www.preprints.org) | NOT PEER-REVIEWED | Posted: 29 June 2023 doi:10.20944/preprints202306.2005.v1

Table 1. Proposed frequency ranges for control tasks.

Frequency Range	Pilot Control Strategy/Task
0.25–0.8 rad/sec (0.04–0.13 Hz)	Typical open-loop control associated with trimming and flight path modulation
0.8–2.0 rad/sec (0.13–0.32 Hz)	Typical closed-loop control associated with transport aircraft maneuvering
2.0–4.0 rad/sec (0.32–0.64 Hz)	Higher-gain closed-loop control associated with increased task urgency or handling issues with the aircraft, such as PIO
4.0–10.0 rad/sec (0.64–1.59 Hz)	Very high-gain closed-loop control, almost certainly associated with control difficulties

By observing the control strategy descriptions corresponding to different frequency component ranges in Table 1, and considering the pilot's handling qualities rating (HQR) based on the Cooper-Harper scale as shown in Figure 5 [10], a correspondence can be found between the two.

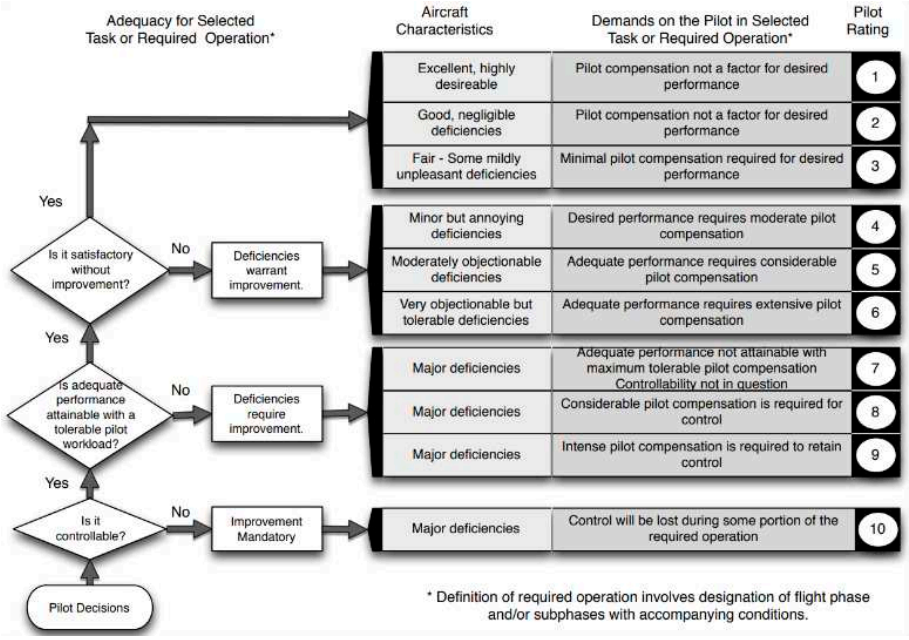

Figure 5. Cooper-Harper Handling Qualities Rating Scale.

By observing the pilot control descriptions in Table 1 and Figure 5, it can be inferred that the frequency range of 0.25-0.8 rad/sec likely corresponds to HQR Level 1 (1~3), the range of 0.8-2.0 rad/sec corresponds to HQR Level 2 (4~6), the range of 2.0-4.0 rad/sec corresponds to HQR Level 3 (7~9), and the flight task description corresponding to the range of 4.0-10.0 rad/sec aligns with an HQR rating of 10.

Therefore, the pilot control workload assessment method can be described as follows: Extract the main frequency components of pilot control actions using wavelet transform. Then, predict the pilot's control workload level and potential rating range based on the mapping relationship between pilot control amplitude, frequency components, corresponding control strategy descriptions, and the Cooper-Harper HQR Scale. This method provides a detailed description of the actual amplitude and frequency of pilot control inputs, while also offering a quantitative measure through the simple HQR rating. This method allows for a more in-depth analysis of the pilot's control characteristics, which is helpful in determining pilot control strategies that are both more reasonable and impose lower control workload.

Preprints (www.preprints.org) | NOT PEER-REVIEWED | Posted: 29 June 2023 doi:10.20944/preprints202306.2005.v1

To enhance the numerical efficiency of the wavelet analysis, a sampling frequency of 20 Hz is chosen, considering that the pilot's control frequencies can be identified up to 10.0 rad/sec (1.6 Hz). After sampling, the initial stick deflection displacement is subtracted since the pilot does not apply any control deflection at the initial state (energy value of 0 for the initial signal). For the wavelet transform, the widely used db3 wavelet function is selected.

5. Tilt-rotor aircraft forward conversion procedure

5.1. Task Description

In this section, we employ the optimal control method established in Section 3 and the pilot workload evaluation method developed in Section 4 to investigate the control strategy for forward conversion of tilt-rotor aircraft and evaluate the pilot workload. The XV-15 tilt-rotor aircraft is taken as the example.

Relevant literature and flight tests [5,15,19] indicate that the initial speed for forward conversion in helicopter mode is generally between 30.6 m/s and 41.7 m/s, corresponding to a low-power state in the helicopter mode. In the final stage of the conversion, the forward flight speed range is typically limited to 61.7 m/s to 72 m/s, corresponding to a low-power state in the fixed-wing mode. Additionally, the rotor speed is maintained at 589 r/min throughout, while the aileron/flap configuration remains at 40°/25°. Once in fixed-wing mode and stabilized, the pilot reduces the rotor speed in order to minimize vibration levels and switches the aileron/flap configuration to 0°/0° to enter high-speed fixed-wing aircraft mode. Therefore, the initial state of conversion is determined as follows: mass of 5897 kg, aft center of gravity, standard atmospheric conditions, no crosswind, steady level forward flight speed of 35 m/s, and altitude of 100 m, a 2-second wait. After conversion, the speed is maintained at 61.7 m/s to 72 m/s in steady-level flight, with the aileron/flap configuration remaining at 40°/25° throughout. The boundary condition can be specified as follows,

$$\begin{cases} i_{\mathrm{n}}(t_{\mathrm{f}}) = 0^{\circ} \\ 61.7\mathrm{m/s} \le \dot{x}(t_{\mathrm{f}}) \le 72\mathrm{m/s}, \dot{h}(t_{\mathrm{f}}) = 0\mathrm{m/s} \\ q(t_{\mathrm{f}}) = 0^{\circ}/\mathrm{s}, \dot{q}(t_{\mathrm{f}}) = 0^{\circ}/\mathrm{s}^2 \\ \dot{u}(t_{\mathrm{f}}) = 0\,m/\mathrm{s}^2, \dot{w}(t_{\mathrm{f}}) = 0\,m/\mathrm{s}^2 \\ u_{\mathrm{n}}(t_{\mathrm{f}}) = 0^{\circ}/\mathrm{s}, u_{\mathrm{col}}(t_{\mathrm{f}}) = 0\%/\mathrm{s}, u_{\mathrm{lon}}(t_{\mathrm{f}}) = 0\%/\mathrm{s} \end{cases} \tag{20}$$

If tilt-rotor aircraft encounters danger in conversion mode, it is unable to quickly make maneuver to avoid it. Besides, it cannot quickly enter into autorotation when the engine fails in conversion mode. Therefore, it is one of the most important indexes to complete the conversion as soon as possible within the safety range. In this section, we will consider the minimum time performance index as the benchmark, and subsequently supplement it with the pilot workload item.

5.2. Benchmark performance index

The benchmark performance index of minimum time is set as

$$\min J_{\mathrm{C1}} = \tau_{\mathrm{f}} - \tau_0 \tag{21}$$

Figure 6 presents the computed results of the forward dynamic conversion control strategy under the benchmark performance index J_{C1}.

Preprints (www.preprints.org) | NOT PEER-REVIEWED | Posted: 29 June 2023 doi:10.20944/preprints202306.2005.v1

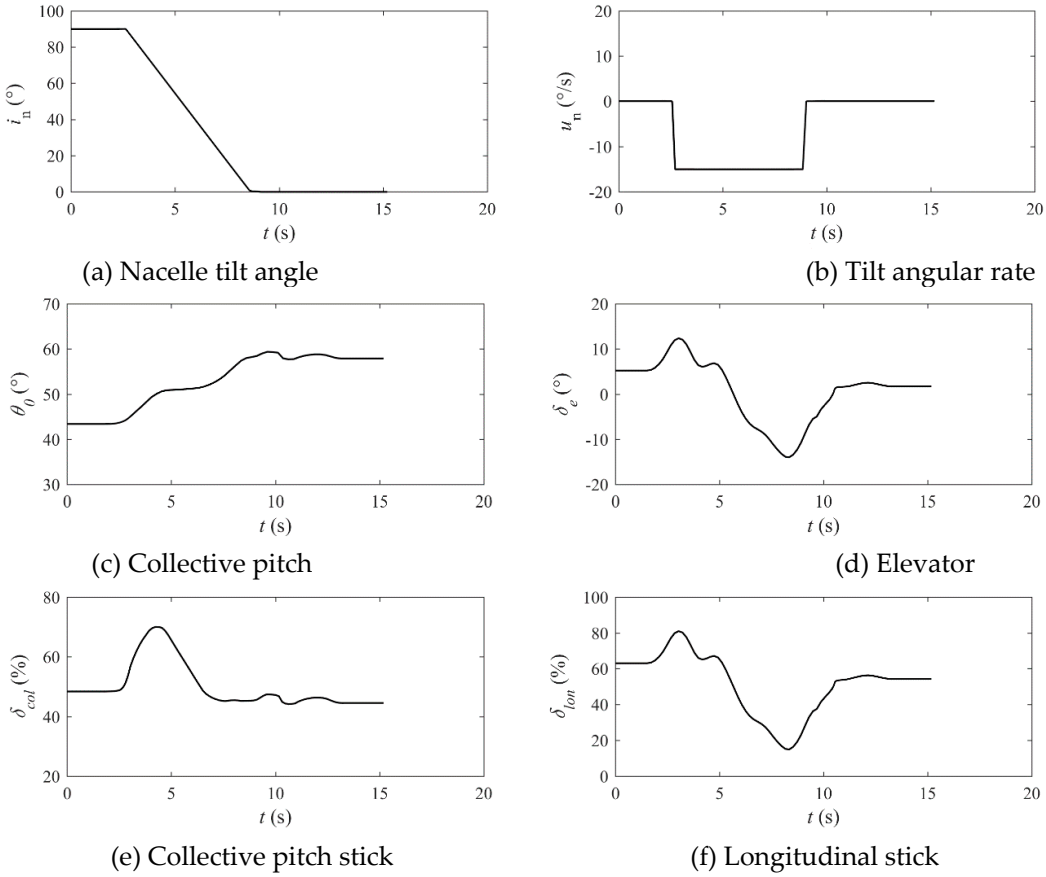

Figure 6. Forward conversion control strategy under benchmark performance index J_{C1}.

As shown in Figure 6, the engine nacelle tilts at a maximum angular rate of 15°/s, taking approximately 6 seconds to tilt into the fixed-wing aircraft mode. However, from Figure 6(b), it can be observed that the engine tilt angular rate experiences a jump between 0°/s and 15°/s at the beginning and end, resulting in a sudden increase in tilt angular acceleration. This is not only detrimental to the design of the tilt control system but also affects the pitch angular acceleration of the aircraft, thereby impacting flight quality. Additionally, the collective pitch stick undergoes a change of 27% in amplitude, with a rate range between -20%/s and 20%/s. The longitudinal stick changes by 66% in amplitude, with a rate jumping between -30%/s and 30%/s, indicating relatively aggressive pilot manipulation.

To further illustrate the level of aggressiveness in pilot manipulation under performance index J_{C1}, the workload evaluation method based on wavelet analysis is applied to the pilot's manipulation of the collective pitch stick and longitudinal stick, followed by an evaluation of the pilot's workload.

Figure 7 presents the wavelet analysis results of the pilot's manipulation actions during forward conversion under benchmark performance index J_{C1}. Figure 7(a) shows the wavelet transform result of the collective pitch stick. It can be observed that there is a high-energy input in the range of 0.2 rad/s to 2.0 rad/s, occurring from 2 s to 6 s. This indicates a significant amplitude of the pilot input. After 12 s, there is also a small-amplitude manipulation around 0.5 rad/s, corresponding to the balancing process of the collective pitch stick. Furthermore, there are some lower-energy (small-amplitude) high-frequency components (exceeding 2 rad/s) present at 4 s, 6 s, and 10 s. These are caused by the continuous jumping of the collective pitch control rate within the constraint range. Figure 7(b) displays the wavelet transform result of the pilot manipulation of the longitudinal stick. Comparing it with Figure 6, it can be observed that the maximum energy input of the longitudinal stick is significantly greater than that of the collective pitch stick. This is due to the more drastic amplitude changes of the longitudinal stick, requiring the pilot to input greater energy for

Preprints (www.preprints.org) | NOT PEER-REVIEWED | Posted: 29 June 2023 doi:10.20944/preprints202306.2005.v1

manipulation. The longitudinal stick exhibits a medium-energy input in the range of 0.2 rad/s to 1.0 rad/s from 2 s to 5 s, while a high-energy input in the range of 0.1 rad/s to 1.5 rad/s occurs from 6 s to 10 s. These frequency components correspond to the pilot adjusting the flight attitude. Additionally, there are some lower-energy (small-amplitude) high-frequency components (exceeding 2 rad/s) present at around 3 s, 5 s, 8 s, and 10 s. These are also a result of the longitudinal stcik control rate continuously jumping within the constraint range.

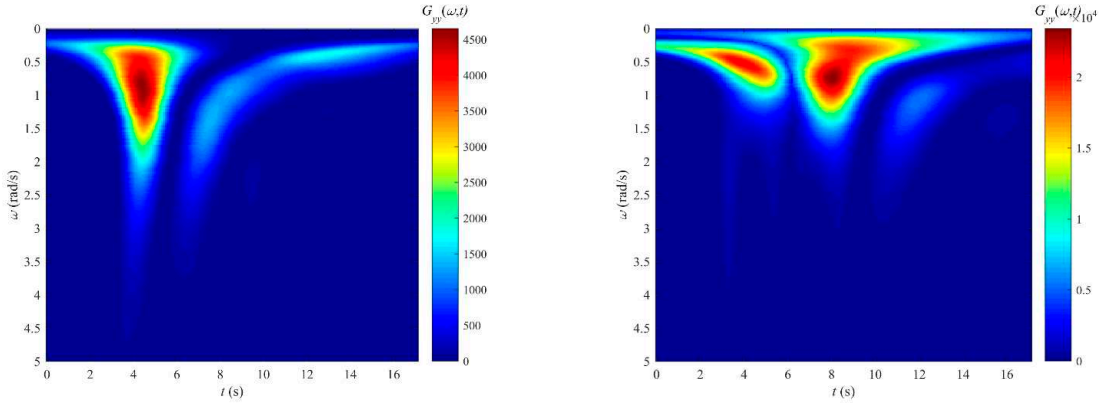

(a) Left, Collective pitch stick wavelet transform result, unit %²/(rad/s)

(b) Right, Longitudinal stick wavelet transform result, unit %²/(rad/s)

Figure 7. Wavelet analysis results of pilot manipulation under benchmark performance index J_{C1}.

Comparing with Table 1, it is evident that the low-frequency, high-energy density components in pilot manipulation primarily correspond to flight path adjustments and conventional maneuvering. On the other hand, high-frequency, low-energy density components pose challenges to flight tasks and may even induce pilot-induced oscillations. According to the pilot control workload assessment method proposed in Section 4, the benchmark performance index J_{C1} indicates a high control workload for forward dynamic conversion corresponding to HQR level 3. This implies a significant control burden, making it difficult for the pilot to achieve a safe and feasible forward conversion process. Therefore, it is necessary to consider the pilot's workload in the performance index to prevent high-frequency jumps in the manipulation rates of the collective pitch stick and longitudinal stick.

5.3. Weighting of pilot workload in performance index

In order to incorporate the pilot workload into the performance index, this section introduces a weighting of the pilot control rate objective component based on the benchmark performance index J_{C1}. Since the limitations of altitude and attitude in the conversion process can be expressed by path constraints according to different missions, the performance index in this paper is set as follows

$$\min J_{C2} = w_t\left(\tau_f - \tau_0\right) + \frac{w_p}{\tau_f - \tau_0}\int_{\tau_0}^{\tau_f}\left[w_{col}\cdot u_{col}^2(\tau) + w_{lon}\cdot u_{lon}^2(\tau) + w_n\cdot u_n^2(\tau)\right]\mathrm{d}\tau \tag{22}$$

The pilot mainly focuses on the control of the collective pitch stick and longitudinal stick in the process of conversion, so the weight coefficients w_{col} and w_{lon} are set higher than w_n. The specific values are selected as w_{lon}=0.5, w_{col}=0.35, w_n=0.15. The distribution of the pilot workload weight coefficient w_p and the time weight coefficient w_t has a great influence on the quality of conversion procedure. Figure 8 shows the pilot control strategy and flight state under different w_p/w_t.

Preprints (www.preprints.org) | NOT PEER-REVIEWED | Posted: 29 June 2023 doi:10.20944/preprints202306.2005.v1

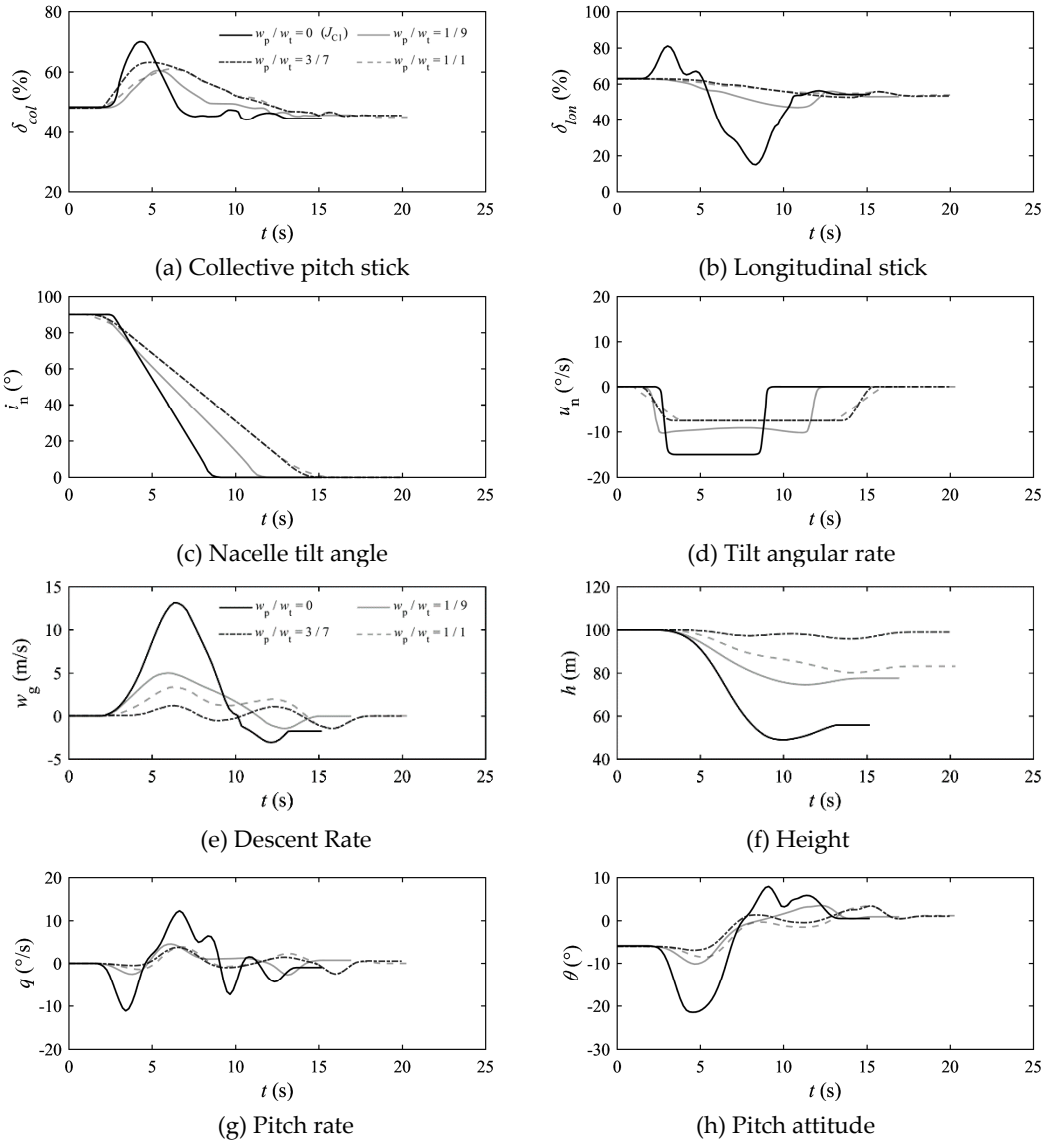

(a) Collective pitch stick (b) Longitudinal stick

(c) Nacelle tilt angle (d) Tilt angular rate

(e) Descent Rate (f) Height

(g) Pitch rate (h) Pitch attitude

Figure 8. Forward conversion in different w_P/w_t under performance index J_{C2}.

As can be seen from Figure 8, when the performance index considers the weight coefficient of pilot workload (w_P), the displacements of controls are significantly reduced, and the height and pitch attitude change more gently, but the time has been extended. In addition, w_P should not be dominant, otherwise the overly smooth manipulation will lead to a decrease of height. When the ratio of w_P/w_t is 3/7 for conversion procedure, the pilot manipulation is smooth, the height change is small, and the tilting process of the engine nacelle can be basically realized by the constant angular rate automatic tilting system (stabilized at 7.5°/s). Therefore, the performance index is set as

$$\min J_{C2} = 0.7\left(\tau_f - \tau_0\right) + \frac{0.3}{\tau_f - \tau_0}\int_{\tau_0}^{\tau_f}\left[w_{col}\cdot u_{col}^2(\tau) + w_{lon}\cdot u_{lon}^2(\tau) + w_n\cdot u_n^2(\tau)\right]\mathrm{d}\tau \tag{23}$$

Figure 9 presents the wavelet analysis results of the pilot's manipulation actions during forward conversion under benchmark performance index J_{C2}.

Preprints (www.preprints.org) | NOT PEER-REVIEWED | Posted: 29 June 2023 doi:10.20944/preprints202306.2005.v1

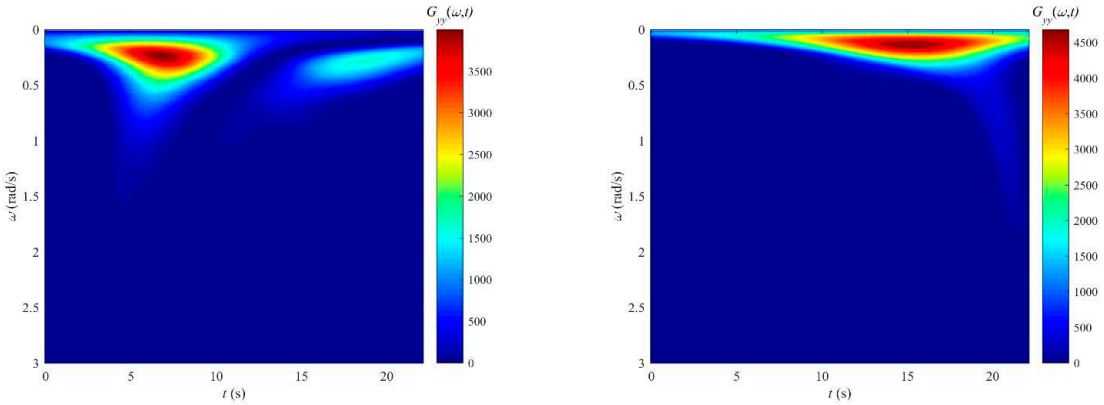

(a) Left, Collective pitch stick wavelet transform result, unit %²/(rad/s)

(b) Right, Longitudinal stick wavelet transform result, unit %²/(rad/s)

Figure 9. Wavelet analysis results of pilot manipulation under performance index J_{C2}.

Figure 9(a) shows the wavelet transform result of the collective pitch stick. It can be observed that the overall energy distribution of the collective pitch stick is similar to that shown in Figure 7(a), but with a 15% decrease in maximum energy input. The main energy inputs are concentrated around 0.1 rad/s to 0.8 rad/s, and the high-frequency components with low energy (small amplitudes) are also below 1.6 rad/s. This is because the performance metric J_{C2} considers the control rate of the collective pitch stick, preventing it from jumping abruptly. Figure 9(b) displays the wavelet transform results of the longitudinal stick. A comparison with Figure 7(b) reveals a significant decrease (80%) in the maximum energy of the longitudinal rod, with the main energy inputs corresponding to frequencies below 0.3 rad/s, representing the pilot's adjustments of the flight attitude. Additionally, the low-energy (small amplitude) high-frequency components appearing after 20 seconds are also below 1.8 rad/s, corresponding to the final trim control process.

Referring to Table 1 provided in Section 4, it can be inferred that the pilot manipulation involves trim and flight path adjustments (with most of the energy inputs corresponding to frequency components below 0.8 rad/s). Only a small portion of the energy inputs correspond to maneuvering actions seen in transport aircraft (frequency components ranging from 0.8 to 2.0 rad/s). Based on the mapping relationship between frequency components and workload proposed in this paper, it is likely that the pilot control workload with the performance metric J_{C2} falls between Level 1 and Level 2 of the HQR scale (rated as 3-4), indicating that the forward conversion a process of low workload and relatively simple and easy manipulation for the pilot.

6. Tilt-rotor aircraft backward reconversion procedure

6.1. Task Description

In this section, we employ the optimal control method established in Section 3 and the pilot workload evaluation method developed in Section 4 to investigate the control strategy for backward reconversion of tilt-rotor aircraft and evaluate the pilot workload. The XV-15 tilt-rotor aircraft is taken as the example.

Based on relevant literature and flight tests [5,15,19], the pilot initiates the deceleration in high-speed fixed-wing mode, simultaneously increasing the rotor speed to 589 r/min and switching the aileron/flap configuration to 40°/25° in preparation for the reconversion. At this stage, the forward flight speed range is generally between 61.7 m/s and 72 m/s (with a tilt angle of the engine nacelle, i_n=0°), corresponding to a low-power state in the fixed-wing mode. In the final stage of the reconversion, the forward flight speed range is typically restricted to 30.6 m/s to 41.7 m/s, corresponding to a low-power state in the helicopter mode. The aileron/flap configuration and rotor speed during remain the same as in the forward convension process. Therefore, the initial state of reconversion is determined as follows: mass of 5897 kg, aft center of gravity, standard atmospheric conditions, no crosswind, steady level forward flight speed of 65 m/s, and altitude of 100 m, a

Preprints (www.preprints.org) | NOT PEER-REVIEWED | Posted: 29 June 2023 doi:10.20944/preprints202306.2005.v1

2-second wait. After backward reconversion, the speed is maintained at 30.6 m/s to 41.7 m/s in steady-level flight, with the aileron/flap configuration remaining at 40°/25° throughout. The boundary condition can be specified as follows,

$$\begin{cases} i_{\mathrm{n}}(t_{\mathrm{f}}) = 90° \\ 30.6\ \mathrm{m/s} \le \dot{x}(t_{\mathrm{f}}) \le 41.7\ \mathrm{m/s} \\ \dot{h}(t_{\mathrm{f}}) = 0\mathrm{m/s} \\ q(t_{\mathrm{f}}) = 0°/\mathrm{s}, \dot{q}(t_{\mathrm{f}}) = 0°/\mathrm{s}^2 \\ \dot{u}(t_{\mathrm{f}}) = 0\,m/\mathrm{s}^2, \dot{w}(t_{\mathrm{f}}) = 0\,m/\mathrm{s}^2 \\ u_{\mathrm{n}}(t_{\mathrm{f}}) = 0°/\mathrm{s}, u_{\mathrm{col}}(t_{\mathrm{f}}) = 0\%/\mathrm{s}, u_{\mathrm{lon}}(t_{\mathrm{f}}) = 0\%/\mathrm{s} \end{cases} \tag{24}$$

Similar to the research process for forward conversion performance index, this section first adopts the minimum time performance index as the primary benchmark, followed by supplementary analysis of the pilot workload item.

6.2. Benchmark performance index

The benchmark performance index of minimum time is set as

$$\min J_{\mathrm{R1}} = \tau_{\mathrm{f}} - \tau_0 \tag{25}$$

Figure 10 presents the computed results of the backward dynamic reconversion control strategy under the benchmark performance index J_{R1}.

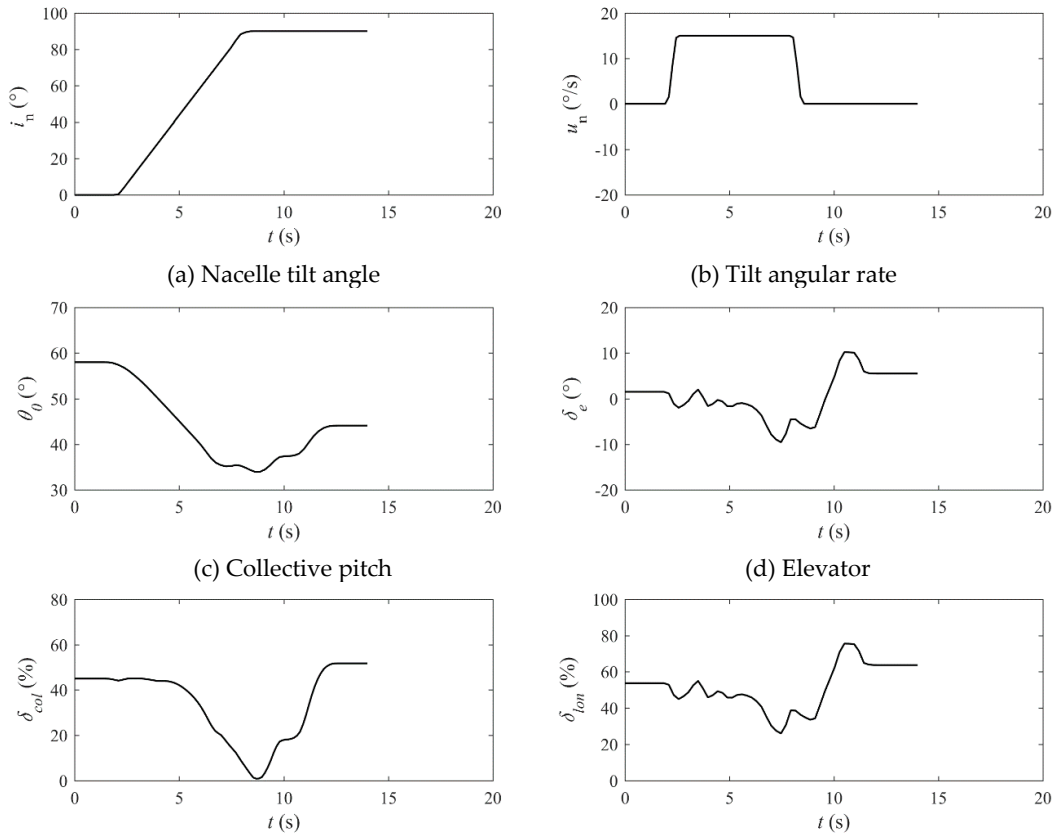

(a) Nacelle tilt angle (b) Tilt angular rate

(c) Collective pitch (d) Elevator

(e) Collective pitch stick (f) Longitudinal stick

Figure 10. Backward reconversion control strategy under benchmark performance index J_{R1}.

From Figure 10, it can be observed that when considering only the time aspect of the performance index, the engine nacelle tilts at a maximum angular rate of 15°/s, requiring approximately 6 seconds to transition back to helicopter mode. However, as depicted in Figure 10(b), there are noticeable jumps in the engine tilt angular rate between 0°/s and 15°/s at the initial

Preprints (www.preprints.org) | NOT PEER-REVIEWED | Posted: 29 June 2023 doi:10.20944/preprints202306.2005.v1

and final stages, resulting in a sudden increase in tilt angular acceleration. Additionally, the collective pitch stick displacement exhibits a significant variation, reaching its minimum point (0%) at 8 s. The longitudinal stick displacement also demonstrates intense fluctuations, with control rate fluctuating between -30%/s and 30%/s.

To further illustrate the level of aggressiveness in pilot manipulation under performance index J_{R1}, the workload evaluation method based on wavelet analysis is applied to the pilot's manipulation of the collective pitch stick and longitudinal stick, followed by an evaluation of the pilot's workload.

Figure 11 presents the wavelet analysis results of the pilot's manipulation actions during backward reconversion control strategy under benchmark performance index J_{R1}. It can be observed that the maximum energy input for the collective pitch stick at approximately 8 s significantly exceeds that of the longitudinal stick, but the high-frequency components are lower compared to those of the longitudinal stick. At 12 s, there is a lower-energy high-frequency component, indicating a sense of urgency in the flight task, as indicated by Table 1. The longitudinal stick, on the other hand, shows numerous small-amplitude high-frequency components distributed vertically across different time nodes. This is caused by the continuous jumps in longitudinal stick control rate within the constraint range, with some exceeding 4 rad/s. It is evident from Table 1 that such control is challenging for the pilot.

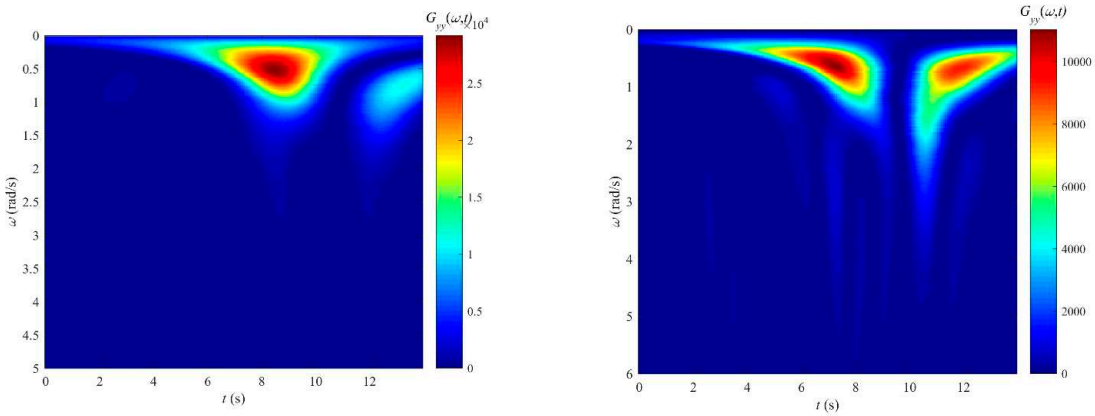

(a) Left, Collective pitch stick wavelet transform result, unit %²/(rad/s)

(b) Right, Longitudinal stick wavelet transform result, unit %²/(rad/s)

Figure 11. Wavelet analysis results of pilot manipulation under benchmark performance index J_{R1}.

According to the mapping relationship between frequency components and control loads proposed in Section 4, the corresponding HQR level for backward reconversion under benchmark performance index J_{R1} indicates level 3, suggesting control difficulty for the pilot. Therefore, it is necessary to consider the pilot's control workload in the performance index to avoid significant manipulation of the collective pitch stick and the presence of high-frequency components in both collective pitch stick and longitudinal stick controls.

6.3. Weighting of pilot workload in performance index

To incorporate the pilot workload into the performance index, this section also introduces the weighted pilot control rate term based on the benchmark performance index J_{R1}. This approach is consistent with Section 5.3.

$$\min J_{C2} = w_t\left(\tau_f - \tau_0\right) + \frac{w_p}{\tau_f - \tau_0}\int_{\tau_0}^{\tau_f}\left[w_{col}\cdot u_{col}^2(\tau) + w_{lon}\cdot u_{lon}^2(\tau) + w_n\cdot u_n^2(\tau)\right]\mathrm{d}\tau \tag{26}$$

The weight coefficients w_{col}, w_{lon} and w_n are also selected as w_{lon}=0.5, w_{col}=0.35, w_n=0.15. The distribution of the pilot workload weight coefficient w_p and the time weight coefficient w_t has a great influence on the quality of conversion procedure. Figure 12 shows the pilot control strategy and

Preprints (www.preprints.org) | NOT PEER-REVIEWED | Posted: 29 June 2023 doi:10.20944/preprints202306.2005.v1

flight state under different w_p/w_t. It can be concluded that when the ratio of w_p/w_t is 1/1 for reconversion procedure, the pilot manipulation is smooth, the height change is small, and the tilting process of the engine nacelle can be basically realized by the constant angular rate automatic tilting system (stabilized at 7.5°/s).

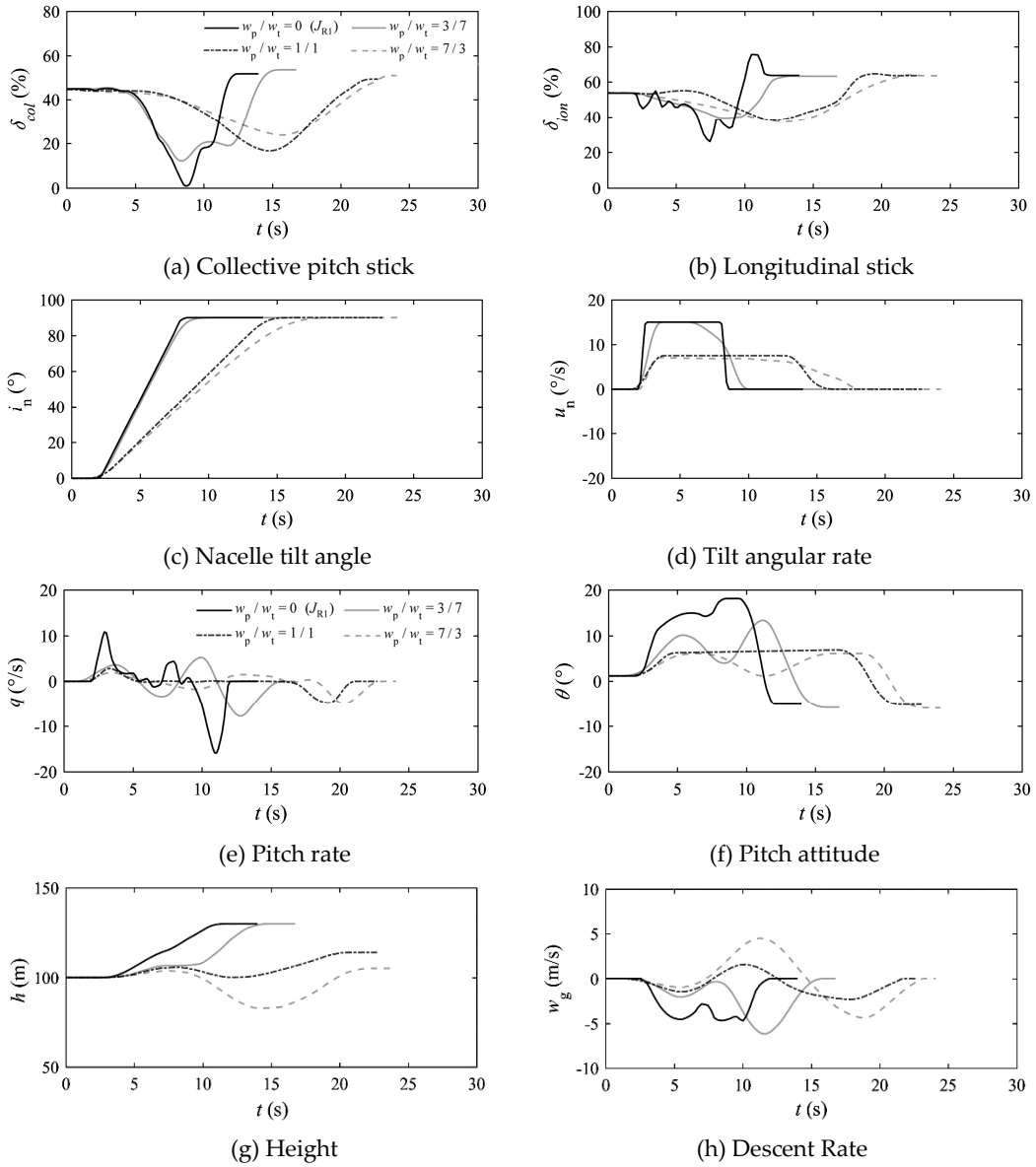

(a) Collective pitch stick (b) Longitudinal stick

(c) Nacelle tilt angle (d) Tilt angular rate

(e) Pitch rate (f) Pitch attitude

(g) Height (h) Descent Rate

Figure 12. Backward reconversion in different w_p/w_t under performance index J_{R2}.

Therefore, the performance index is set as

$$\min J_{R2}=0.5\left(\tau_f-\tau_0\right)+\frac{0.5}{\tau_f-\tau_0}\int_{\tau_0}^{\tau_f}\left[w_{col}\cdot u_{col}^2(\tau)+w_{lon}\cdot u_{lon}^2(\tau)+w_n\cdot u_n^2(\tau)\right]\mathrm{d}\tau \tag{27}$$

Figure 13 presents the wavelet analysis results of the pilot's manipulation actions during backward reconversion under benchmark performance index J_{R2}.

Preprints (www.preprints.org) | NOT PEER-REVIEWED | Posted: 29 June 2023 doi:10.20944/preprints202306.2005.v1

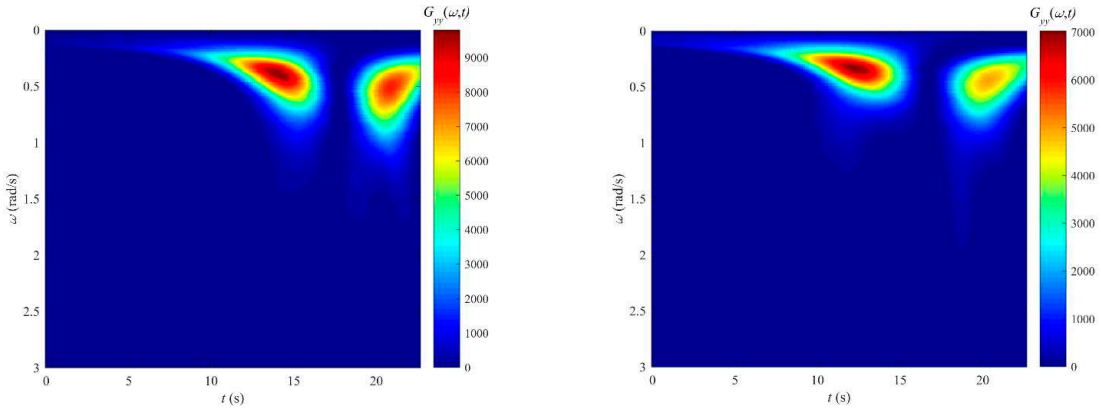

(a) Left, Collective pitch stick wavelet transform result, unit %²/(rad/s)

(b) Right, Longitudinal stick wavelet transform result, unit %²/(rad/s)

Figure 13. Wavelet analysis results of pilot manipulation under performance index J_{R2}.

Figure 13(a) shows the wavelet transform result of the collective pitch stick. It can be observed that the overall energy distribution of the collective pitch stick is similar to that shown in Figure 11(a) , but the maximum energy input has significantly reduced by 66%. The main energy inputs are concentrated around 0.2 rad/s to 0.8 rad/s, and the low-energy (small-amplitude) high-frequency components are also less than 1.7 rad/s. Figure 13(b) displays the wavelet transform result of the longitudinal stick. A comparison with Figure 11(b) reveals a 36% decrease in the maximum energy of the longitudinal stick and a significant reduction in high-frequency components. The low-energy (small-amplitude) high-frequency components that appear after 12 s and 18 s are also less than 2 rad/s.

Referring to Table 1, it can be concluded that the pilot manipulation mainly involves trim and flight path adjustments (with most of the energy inputs corresponding to frequency components below 0.8 rad/s). There is only a small degree of manipulation associated with transport aircraft maneuvers (a tiny portion of energy inputs corresponding to frequency components between 0.8 and 2.0 rad/s). According to the pilot control workload assessment method proposed in Section 4, it can be inferred that the pilot control workload with performance index J_{R2} corresponds to Level 1~2 (HQR 3~4). This indicates that the backward reconversion is a process of low workload and relatively simple and easy manipulation for the pilot.

7. Conclusions

This paper studies the control strategies and workload of tilt-rotor aircraft dynamic conversion and reconversion procedures. A nonlinear flight dynamics model of tilt-rotor aircraft with full flight modes is established. On this basis, a nonlinear optimal control model of dynamic conversion is constructed. An analytical method based on wavelet transform is proposed, which examines the mapping relationship between pilot control input's amplitude, constituent frequencies, and control tasks. The investigations yielded the following conclusions.

1) When the performance index considers the weight coefficient of pilot workload, the magnitude of collective stick inputs and longitudinal stick inputs are significantly reduced, while promoting smoother changes in height and pitch attitude. Additionally, the tilting of the engine nacelle can be accomplished at a lower and fixed angular rate. However, the pilot workload weight coefficient should not be too dominant, otherwise the overly smooth collective stick and longitudinal stick manipulation will lead to a decrease of height.

2) By incorporating the nonlinear optimal control model and the pilot workload evaluation method, this study proposes control strategies for both forward conversion and backward reconversion with low pilot workload. Through the utilization of appropriate performance indexes, it is estimated that both the conversion and reconversion procedures exhibit a low workload level (HQR 3~4, Level 1~2), making them relatively straightforward and easily manageable for the pilot.

8. Future Works

In order to further enhance the numerical simulation accuracy of dynamic conversion process and improve the accuracy of pilot workload evaluation, further development and refinement of the pilot workload evaluation method is needed. The mapping relationship between the pilot's control amplitudes, frequency components, and pilot workload requires further validation and adjustment through flight experiments and simulations. Additionally, it would be beneficial to develop a pilot model that accurately reflects the pilot's workload, enabling a more precise evaluation of pilot workload during flight simulations.

Author Contributions: Conceptualization, X. Y. and R. C.; methodology, X. Y.; software, X. Y.; validation, X. Y., R. C. and Y. Y.; formal analysis, Y. Y.; investigation, X. Y.; resources, R. C.; data curation, X. Y.; writing—original draft preparation, X. Y.; writing—review and editing, X. Y. and Y. Y.; supervision, Y. Y.; project administration, X. Y. and R. C.; funding acquisition, X. Y. All authors have read and agreed to the published version of the manuscript.

Funding: The research is supported by the National Natural Science Foundation of China (No. NSFC-12202406), and the Natural Science Foundation of China (No. 11672128).

Data Availability Statement: The data that support the findings of this study are available from the corresponding author upon reasonable request.

Conflicts of Interest: The authors declare no conflicts of interest.

References

1. Yuan, Y.; Thomson, D.; Anderson, D. Application of Automatic Differentiation for Tilt-Rotor Aircraft Flight Dynamics Analysis, *J. Aircr*. **2020**, *57* (5), pp. 985-990. https://doi.org/10.2514/1.C035811
2. Xufei, Y.; Renliang, C. Augmented flight dynamics model for pilot workload evaluation in tilt-rotor aircraft optimal landing procedure after one engine failure. *Chin. J. of Aeronaut.* 2019, *32*(1), pp. 92-103. https://doi.org/10.1016/j.cja.2018.06.010
3. Padfield, G. D. *Helicopter flight dynamics: including a treatment of tiltrotor aircraft*, 3rd ed.; John Wiley & Sons: New York, USA, 2018; pp.154-196.
4. Nabi, H.; De, V. C.; Pavel, M. D., et al. A quasi-linear parameter varying (qlpv) approach for tiltrotor conversion modeling and control synthesis. In Proceedings of the American Helicopter Society 75th Annual Forum, AHS, Philadelphia, USA, 13–16 May 2019; pp. 1-12.
5. Yan, X.; Chen, R.; Lou, B., et al. Study on control strategy for tilt-rotor aircraft conversion procedure. *Journal of Physics: Conference Series*. **2021**, *1924*(1), pp. 012010. https://doi.org/10.1088/1742-6596/1924/1/012010.
6. Yeo, H.; Saberi, H. Tiltrotor conversion maneuver analysis with RCAS. *J Am Helicopter Soc*. **2021**, *66*(4), pp. 1-14. https://doi.org/10.4050/JAHS.66.042010
7. Righetti, A.; Muscarello, V.; Quaranta, G. Linear parameter varying models for the optimization of tiltrotor conversion maneuver. In Proceedings of the American Helicopter Society 73th Annual Forum, AHS, Fort Worth, USA, 9–11 May 2017; pp. 280-287.
8. Memon, W. A.; White, M. D.; Padfield, G. D., et al. Helicopter Handling Qualities: A study in pilot control compensation. *Aeronaut J*. **2022**, *126*(1295), pp. 152-186. https://doi.org/10.1017/aer.2021.87
9. Bachelder, E. N.; Aponso, B. L.; Berger, T. A Theoretical Basis for Predicting Pilot Performance, Workload, and Handling Qualities. In Proceedings of AIAA SCITECH 2023 Forum, AIAA, National Harbor, MD & Online, 23-27 January 2023; pp. 1369. https://doi.org/10.2514/6.2023-1369
10. Bachelder, E. N.; Lusardi, J.; Aponso, B. Estimating Handling Qualities Ratings from Hover Flight Data Using SCOPE. In Proceedings of AIAA Scitech 2021 Forum, AIAA, VIRTUAL EVENT, 11–15 & 19–21 January 2021; pp. 0593. https://doi.org/10.2514/6.2021-0593
11. Klyde, D. H.; Pitoniak, S. P.; Schulze, P. C.; et al. Piloted simulation evaluation of tracking mission task elements for the assessment of high-speed handling qualities. *J Am Helicopter Soc.* **2020**, *65*(3), pp. 1-23. https://doi.org/10.4050/JAHS.65.032010
12. Mello, R. S.; Klyde, D. H.; Mitchell, D. G. Aircraft Accident Investigation Using Wavelet Scalogram-Based Metric to Identify Possible PIO Signature. In Proceedings of AIAA SCITECH 2023 Forum, AIAA, National Harbor, MD & Online, 23-27 January 2023; pp. 1367. https://doi.org/10.2514/6.2023-1367

13. Ji, H.; Chen, R.; Li, P. Real-time simulation model for helicopter flight task analysis in turbulent atmospheric environment, *Aerosp. Sci. and Technol*. 2019, *92*, pp. 289-299. https://doi.org/10.1016/j.ast.2019.05.06
14. Ferguson, S. W. A mathematical model for real time flight simulation of a generic tilt-rotor aircraft. Technical Report: CR-166536, NASA Ames Research Center, 1988.
15. Ferguson, S. W. Development and validation of a simulation for a generic tilt-proprotor aircraft. Technical Report: CR-166537, , NASA Ames Research Center, 1989, pp A1-A185.
16. An, K.; Guo, Z.; Xu, X.; et al. A framework of trajectory design and optimization for the hypersonic gliding vehicle. *Aerosp. Sci. and Technol*. **2020**, *106*, pp. 106110. https://doi.org/10.1016/j.ast.2020.106110
17. Jin, R., Huo, M., Xu, Y., et al. Rapid cooperative optimization of continuous trajectory for electric sails in multiple formation reconstruction scenarios. *Aerosp. Sci. and Technol*. **2023**, pp. 108385. https://doi.org/10.1016/j.ast.2023.108385
18. Yan, X.; Chen, R.; Zhu, S.; et al. Optimal Landing of Tilt-rotor Aircraft after Engine Failure Considering Pilot Inherent Limitations. In Proceedings of 2022 IEEE International Conference on Robotics and Biomimetics (ROBIO), IEEE, Jinghong, China, 05-09 December 2022; pp. 2022: 1036-1040. https://doi.org/10.1109/ROBIO55434.2022.10011647
19. Yu, X.; Chen, R.; Wang, L.; et al. An optimization for alleviating pilot workload during tilt rotor aircraft conversion and reconversion maneuvers. *Aerosp. Sci. and Technol*. **2022**, 129, pp. 107854. https://doi.org/10.1016/j.ast.2022.107854
20. Zhiming, Y.; Xufei, Y.; Renliang, C. Prediction of pilot workload in helicopter landing after one engine failure. *Chin. J. of Aeronaut.* **2020**, *33* (12) , pp. 3112-3124. https://doi.org/10.1016/j.cja.2020.05.021
21. Gossler, F. E.; Oliveira, B, R.; Duarte, M.; et al. Gaussian and Golden Wavelets: A Comparative Study and their Applications in Structural Health Monitoring. *Trends Comput. Appl. Math*. **2021**, *22*, pp. 139-155. https://doi.org/10.5540/tcam.2021.022.01.00139
22. Da, Silva, P. C. L.; Da, Silva, J. P.; Garcia, A. R. G. Daubechies wavelets as basis functions for the vectorial beam propagation method. *J Electromagnet Wave*. **2019**, *33*(8), pp. 1027-1041. https://doi.org/10.1080/09205071.2019.1587319
23. Tritschler, J. K.; O'Connor, J. C.; Holder, J. M.; et al. Interpreting time-frequency analyses of pilot control activity in ADS-33E mission task elements. In Proceedings of American Helicopter Society 73rd Annual Forum, AHS, Fort Worth, USA, 9-11 May 2017.